Journal of Solid State Chemistry 331 (2024) 124547

Contents lists available at ScienceDirect

Journal of Solid State Chemistry

journal homepage: www.elsevier.com/locate/jssc

Nano-strand formation in CaF_2-SiO_2-Al_2O_3-MgO flux reacted at 1350 °C with Al-Ti-Fe powder: SEM analyses and gas reaction thermochemistry

T. Coetsee *, F.J. De Bruin

Department of Materials Science and Metallurgical Engineering, University of Pretoria, Pretoria, 0002, South Africa

ARTICLE INFO

Keywords:
Welding
Thermochemistry
Fluoride
Slag
Gas
Oxy-fluoride

ABSTRACT

Nano-strands form in fluoride-based slag during submerged arc welding (SAW) due to the re-condensation of gas species formed at high temperatures in the arc cavity. The SAW process is complex due to gas-slag-metal reactions occurring across several reaction zones and over a wide temperature range. This complicates research on specific process aspects, such as gas formation from the oxy-fluoride slag. The objective of this work is to demonstrate that oxy-fluoride nano-strands form in molten flux reacted with Al-Ti-Fe metal powder, even at the low temperature of 1350 °C, which is much lower than SAW process temperatures of 2000 °C–2500 °C. Energy dispersive X-ray spectroscopy (EDS) analyses and thermochemical calculations provide insights into formation reactions in nano-strand formation. Thermochemical analysis clarifies the role of Al in shifting the gas phase composition to limit Ti-fluoride loss to the gas phase. These results motivate the study of gas phase reactions at relatively lower reaction temperatures to gain insights into SAW flux behaviour.

1. Introduction

The submerged arc welding (SAW) process is illustrated in cross-section in Fig. 1. In this welding process, an electrical current is applied between the weld wire and the steel base plate to form the arc. Raw granular unmelted flux (flux) and molten flux (slag) cover the arc to form the arc cavity. During welding, the welding head arrangement continuously feeds the weld wire and flux as it moves along the weld. Molten weld wire metal droplets are transferred across the arc cavity into the weld pool. The complex gas phase reactions occur in the arc plasma in the arc cavity and set the conditions for oxygen and alloying element transfer from the slag and weld wire to the weld pool.

Gas phase reactions must be considered in the process metallurgy of SAW because gas phase formation and gas reactions occur at a fast rate at the high temperature of the arc plasma in the arc cavity. The arc plasma temperatures may range from 2000 °C to 2500 °C, and the weld pool temperature can vary from 2000 °C to the solidus temperature of the particular weld metal [1,2]. Detailed experimental work established that oxides in the CaF_2 containing oxide-based welding flux decompose in the arc cavity to release oxygen [3–5]. Metals of high oxygen affinity, such as Ti, Cr and Al, are easily oxidised in the arc cavity and are not easily transferred across the arc [6]. In the conventional SAW process, the weld metal is typically alloyed from TiO_2 in the molten flux (slag) with a maximum Ti alloying content of 410 ppm achieved [7,8]. The gas-slag-metal equilibrium model of the conventional SAW process confirmed the likely gas phase species formed at 2000 °C from a TiO_2 containing flux. The major gas species were identified as CO, NaF, KF, AlF_3, AlF_2, $NaAlF_4$, TiF_3, $KAlF_4$, and the minor gas species (at less than 1 vol %) as Na, K, Mg, CaF_2, MgF_2, MgF, AlF, Mn, Fe, MnF_2, SiF_4, and SiO [9]. The same gas-slag-metal equilibrium model was used to show that increased TiO_2 in the flux formulation did not increase Ti element transfer to the weld metal because of the significant loss of Ti to the arc cavity gas as TiF_3 [7].

In recent work, the SAW process was modified by aluminium-assisted alloying of the weld metal to increase the weld metal Ti content beyond 410 ppm Ti. This enhanced Ti alloying was achieved while maintaining the weld metal ppm O content within acceptable levels for optimum materials properties. Aluminium metal powder was applied as a de-oxidiser element in combination with unconstrained pure metal powders to alloy the carbon steel weld metal [10,11]. The term unconstrained format means that the metal powder is not contained in a metal tube as is the case for metal cored and flux cored wires. The added aluminium de-oxidiser lowered the partial oxygen pressure in the arc cavity and also at the slag-weld pool interface to prevent oxidation of Ti to its oxides, thus avoiding the loss of Ti to the slag [10,11]. The effect of added Al in SAW is similar in combination with Cr or Ti because the

* Corresponding author.
E-mail address: theresa.coetsee@up.ac.za (T. Coetsee).

https://doi.org/10.1016/j.jssc.2024.124547
Received 16 November 2023; Received in revised form 30 December 2023; Accepted 2 January 2024
Available online 3 January 2024

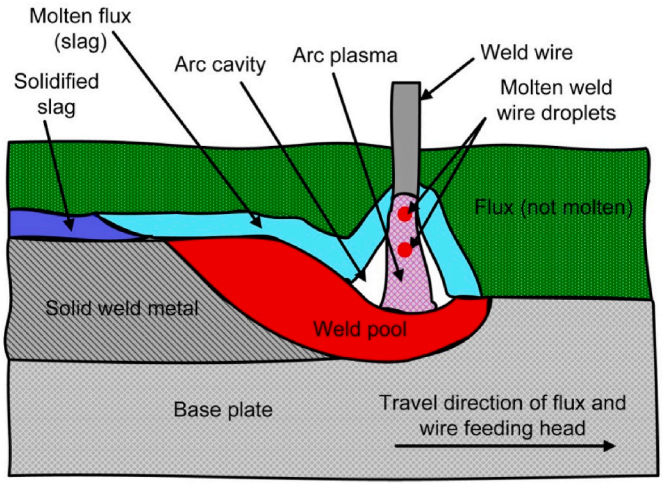

Fig. 1. Illustration of SAW process reaction zones.

added Al metal powder counters the loss reaction of Cr-fluoride and Ti-fluoride gas formation by forming Al-fluorides by preference [12–15]. The formation of oxy-fluoride gas in SAW was confirmed from thermochemical calculations and SEM (scanning electron microscope) identification of the phenomenon of oxy-fluoride nano-strand formation within the cavities within the post-weld slag [12–15]. It was concluded that the nano-strands formed from the re-condensation of the gas species from the initial gas generated in the arc cavity during aluminium-assisted SAW [12–15].

Low temperature fluoride gas formation is known to occur upon heating of fluoride containing casting powders and fluoride containing slags applied in ESR (electro slag remelting) [16–19]. The sequence of fluoride gas species formation upon heating of CaF_2-SiO_2-CaO-Al_2O_3--Na_2O-K_2O mould powders was measured as NaF formation starting at 600 °C, KF formation starting at 883 °C, then SiF_4 and AlF_3 formed upon further heating beyond 830 °C and 974 °C, respectively. CaF_2 vaporisation occurred at higher temperatures beyond 1262 °C. In addition, the following gas species were also measured: $NaAlF_4$, Na_2AlF_5, BF_3, and AlOF [18]. Increased vaporisation with increased TiO_2 content in the CaF_2-CaO-Al_2O_3-MgO-Li_2O-TiO_2 slag was measured in ESR slags reacted at 1470 °C–1530 °C [19]. These studies show that low temperature vaporisation from the oxy-fluoride melt takes place in the form of various gas species in addition to the input fluoride chemical, CaF_2.

The objective of this work is to demonstrate that oxy-fluoride nano-strands form in molten SAW flux reacted with Al-Ti-Fe metal powder at the lower temperature of 1350 °C, which is much lower than SAW process temperatures of 2000 °C–2500 °C [1,2]. The presence of oxy-fluoride nano-strands serves as confirmation of oxy-fluoride vaporisation and re-condensation, similar to that identified in SAW post-weld slags [12–15]. The presence of Ti in the oxy-fluoride nano--strands serves as additional confirmation of the vaporisation and re-condensation of the added Ti metal powder in this reaction system. These results will motivate the study of gas phase reactions at relatively lower reaction temperatures to gain insights into the SAW flux behaviour.

2. Material and methods

The agglomerated commercial flux used in this work is the same formulation applied previously in SAW experiments [9–15]. The flux chemical composition is shown in Table 1 [9–15]. This flux is an Aluminate Basic flux, which was extensively characterised in terms of the mineralogy of both the unreacted flux and its post-weld slag [20]. The expected phase chemistry of this flux upon melting is liquid oxy-fluoride as the primary phase and spinel crystals ($MgO.Al_2O_3$) as the secondary phase [20].

The pure metal powders were sourced as follows: Al (99.7 % Al, -1 mm) supplied by Sigma-Aldrich, Ti (99.5 % Ti, -100 μm) supplied by PLS Technik GmbH & Co., Fe (96.0 % Fe, -50 μm) supplied by Merck. Iron powder was added to simulate the presence of iron from the weld wire and base plate in the prior SAW runs [9–14]. These Al and Ti powders correspond to the Al and Ti metal powders applied in the previous aluminium-assisted SAW work [10–15].

For this study, the flux and metal powders were mixed and dry-pressed into a cylindrical pellet. Each metal powder was added at eight mass% of the overall mixture. The pellet was placed onto the holder made of a low carbon steel plate of 65 mm square and 2 mm thick, with a pressed circular recessed centre. A muffle furnace was pre-heated to 1350 °C. After soaking the muffle furnace for 12 h at 1350 °C, the pellet holder and pellet were placed into the muffle furnace and reacted for 6 min. The pellet was removed from the furnace to cool down in air. The cooled pellet was sectioned through its middle and placed into the SEM to perform phase chemical analyses, following coating with gold. The SEM equipment consisted of a Zeiss crossbeam 540 FEG (field emission gun) SEM with an energy dispersive X-ray (EDS) spectroscopy probe operated at 20 kV.

3. Results and discussion

The presence of nano-strands in the reacted pellet samples is confirmation of gas phase reactions at the relatively low reaction temperature of 1350 °C, compared to the high arc cavity temperatures of 2000 °C–2500 °C in SAW [1,2]. The element distribution in the nano-strands provides analytical data, which is then applied to investigate the likely nano-strand formation reactions. FactSage 7.3 thermochemical software was used to calculate the relative thermodynamic probability of the gas phase reactions occurring [21]. The SEM observations and analyses are presented in the next section (3.1.). The thermochemical analysis of possible reactions is shown in the subsequent section (3.2.).

3.1. SEM analyses

The low magnification (x546) SEM image in Fig. 2(a) clearly shows the presence of nano-strands at the outer edges of the slag ridge. The EDS element maps of the field of view (FOV) in Fig. 2(a) are shown in Fig. 2 (b) and confirm the presence of Ti in the slag at both the nano-strand positions and in the background slag. The element distribution is not homogenous as is expected from a multi-phase slag. The average chemical analysis of the FOV in Fig. 2 is shown in Table 2. For comparison purposes, the flux chemical composition from Table 1 is shown in the last row of Table 2. Although Ti was added as a metal powder of -100 μm particle size to the flux, it is seen that Ti was chemically assimilated into the oxy-fluoride slag in the short reaction time applied. This observation on the assimilation of Ti agrees with the post-weld slag analyses in the same reaction system in which Ti assimilate into the oxy-fluoride slag and not into the spinel crystals [22].

The association of Fe, Mn, and Si as oxy-fluoride is seen in Fig. 2(b). Figs. 3 to 5 display the blocked areas at increased magnification with the

Table 1
Chemical composition of flux material.

%MnO	%CaO	%SiO_2	%Al_2O_3	%CaF_2	%MgO	%Fe_2O_3	%TiO_2	%Na_2O	%K_2O
7.0	0.1	20.2	25.7	18.5	22.9	2.8	1.0	1.7	0.2

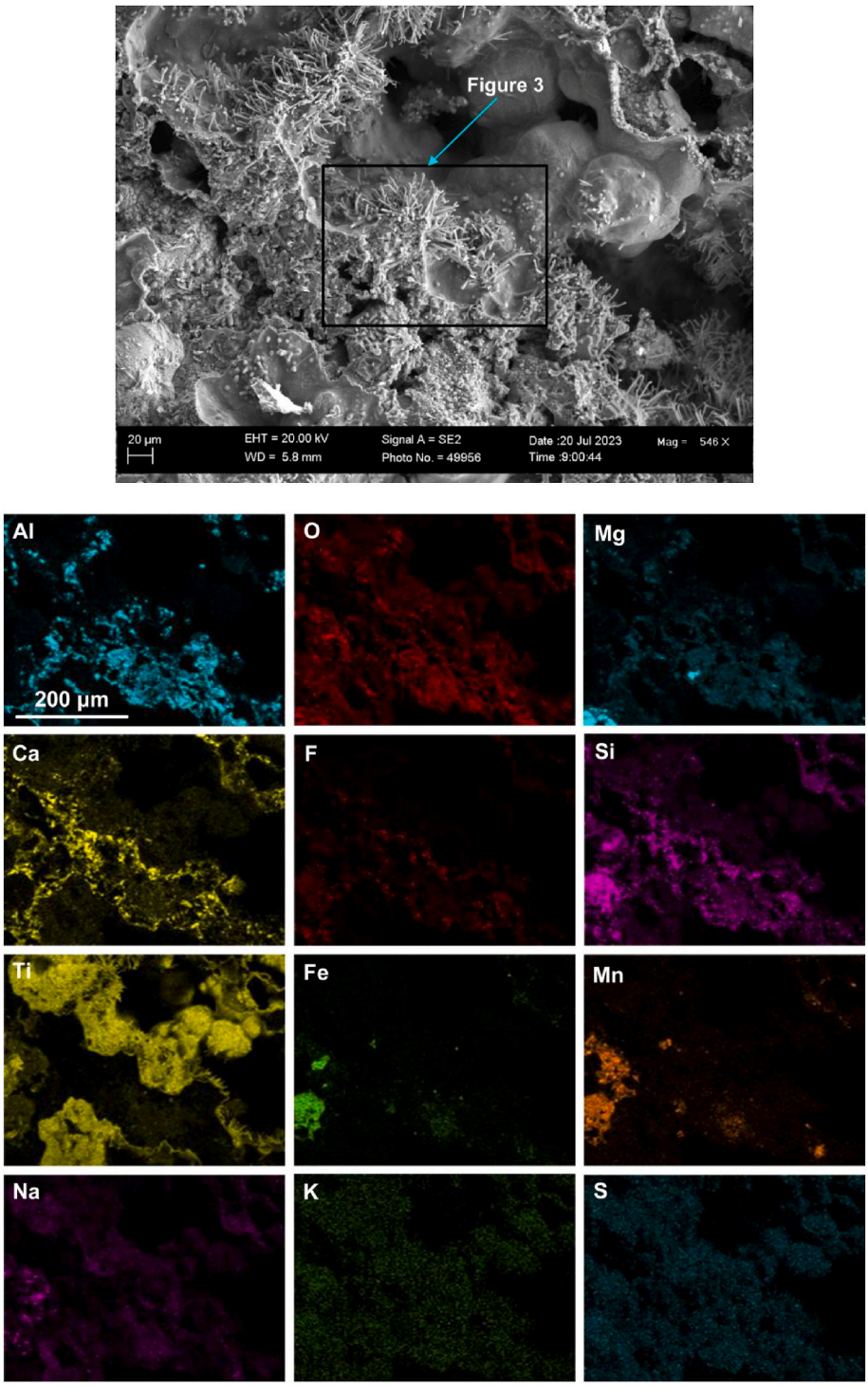

Fig. 2(a). SEM image (x546) of analysed area; (b): EDS map of area in Fig. 2(a).

EDS element maps for each image FOV. The average chemical analyses are summarised in Table 2. The average analyses for the FOV in Figs. 3–5 are similar and not that different from the analysis for the FOV in Fig. 2. Therefore, the EDS element maps are more useful in displaying the element behaviours. It is seen from Fig. 3(b) at (x1580) that the underlying slag phase below the nano-strands consists of Ca-Si-K oxy-fluoride slag with embedded Al-F-O solid phase (spinel phase). The nano-strands contain Ti-O-N-Na, although the presence of fluoride species is unclear at this magnification. At,higher magnification of (x4410) in Fig. 4 and (x7820) in Fig. 5, it is seen that a spinel crystal (triangular shape) is positioned on the slag surface, which spans the left boundary of the image. In Fig. 4, it is seen that fine needle-shaped nano-strands are meshed between the coarser Ti-containing nano-strands and contain most of the elements displayed in the EDS maps, excluding Si, Fe Mn and K. The coarser nano-strands in Fig. 5(b) contain all the elements displayed in the EDS maps with high Ti map intensity. The presence of these nano-strands on the spinel crystal surface agrees with nano-strand formation from the gas phase following vaporisation and re-condensation of oxy-fluoride gas species [12–15]. The N analysed in the nano-strands appear to be superficial and not consistent throughout

Table 2
Average EDS analysis (mass%) of the field of view in Figs. 2 to 10.

Figure	%O	%F	%Na	%Mg	%Al	%Si	%K	%Ca	%Ti	%Mn	%Fe
2	44.3	3.9	3.3	5.8	5.2	2.0	0.1	4.5	27.2	2.2	1.4
3	44.7	4.0	3.2	4.8	4.5	1.4	0.1	4.2	31.9	0.7	0.4
4	43.2	2.2	2.9	3.7	4.0	1.0	0.0	3.2	38.8	0.5	0.4
5	43.3	2.1	3.0	3.5	3.0	1.1	0.1	3.9	39.2	0.5	0.1
6	47.1	5.0	4.4	8.0	8.1	3.3	0.1	4.5	16.6	2.1	0.9
7	49.2	3.5	5.0	7.4	8.2	2.7	0.1	4.4	17.1	1.8	0.4
8	51.4	1.5	7.0	5.9	6.4	1.6	0.0	2.8	21.4	1.6	0.4
9	49.6	0.9	7.8	4.8	4.3	1.7	0.0	3.3	24.8	1.9	0.7
10	49.6	0.9	9.1	4.3	3.2	1.7	0.0	3.3	25.4	1.8	0.4
Flux	35.3	8.7	0.6	13.4	13.2	9.2	0.2	9.3	0.6	5.3	4.2

the EDS analyses since it was not reported in the analysis table as a mass % number. The only source of N is air pockets in the initial pellet; therefore, some nitrogen adsorption is possible.

Figs. 6 to 10 display the slag morphology and phase chemistry at a different analysis area in the same sample. The appearance of the Ti-containing nano-strands is similar to that of Figs. 2 to 5. The average FOV chemical analyses for Figs. 6 to 10 are also displayed in Table 2 and confirm the assimilation of Ti into the slag.

The low magnification (x651) image in Fig. 6 shows that the Ti-containing nano-strands formed on the surface of the slag, similar to the nano-strand morphology displayed in Fig. 2(a). The association of Fe, Mn and Si as oxy-fluoride is similar in Figs. 2(b) and 6(b). Fig. 6(b) also shows the clear slag surface boundary at which the low Ti underlying slag meets the high Ti areas dominated by the Ti-containing nano-strands. Figs. 7 to 10 display the blocked areas at increased magnification with the EDS element maps for each image FOV. Fig. 7(b) at (x1060) magnification shows the incorporation of Mn in the Ti-rich nano-strands. Fig. 8(a) at (x3160) shows similar needle-shaped oxy-fluoride nano-strands to that in Fig. 4. The background slag phase in Fig. 8, as seen in the top half of the FOV, consists of Al-Mg-Ca-Si-Fe-Mn-K-S oxy-fluoride with little to no Ti, Fe, Mn and Na. The Ti-containing nano-strands consist of Al-Mg-Si-Ti-Na oxy-fluoride and are shown more clearly in the higher magnification images in Figs. 9(b) and 10(b) at (x8060) and (x20 000), respectively.

The results in Figs. 2 to 10 confirm that Ti-rich nano-strands formed at the relatively low reaction temperature of 1350 °C. The same analysis techniques applied here were used in prior work to identify and explain gas phase based nano-strand formation in SAW post-weld slags [12–15]. The following observations are strong indicators for nano-strand formation from the gas phase, not the slag. The primary source of Ti is the added Ti metal powder of -100 μm size and not the unreacted flux, as is seen from the raw flux composition in Table 1 and the last line in Table 2. If the nano-strands are formed only from diffusion in the slag phase, the nano-strand distribution should be even across all slag surfaces. This is not observed. The transfer of Ti from the Ti metal powder of -100 μm size to form nano-scale structures seems to be better explained by gas phase transfer, compared to the incorporation of Ti metal into the slag phase and subsequent nano-strand formation by diffusion from the slag. Gas phase diffusion rates are orders of magnitude faster than ionic diffusion rates in slags. For comparison, the gas phase diffusion coefficient is 1 to 6 cm^2/s at 800 °C vs. the ionic diffusivity values for Si^{4+} and O^{2-} in silicate slags at 4 x 10^{-7} cm^2/s to 1 x 10^{-6} cm^2/s at 1600 °C [23, 24]. As seen in Fig. 5, distinct nano-strands are positioned on the spinel crystal surface with no connecting continuous slag layer. The underlying spinel crystal contains no Ca, F, Ti, Na, or Si, meaning that the nano-strands could not have sourced these elements from the underlying spinel crystal.

3.2. Thermochemical analysis

Thermochemistry calculations are used in the following two sections to probe the likely gas phase reactions formed in the reaction of the oxy-fluoride slag and added metal powders of Al, Ti and Fe. Section 3.2.1. contains Gibbs free energy calculations on simplified reactions. Section 3.2.2. contains the application of gas-slag-metal equilibrium calculations to better simulate the interactions between the slag and the added metal powders to form gas species.

3.2.1. Thermochemical analysis of simplified reactions

Ti-fluorides transform from solid to gas at relatively low temperatures at 1102.46 °C for TiF_2, 1033.94 °C for TiF_3 and 284.06 °C for TiF_4. Similarly, AlF_3 transforms from solid to gas at 1290.23 °C, whilst AlF and AlF_2 are reported as gasses in the FactSage 7.3 databases [21]. The Gibbs free energy data in Fig. 11 for reaction (1) shows the relative stability of fluoride compounds, expressed per mol $F_2(g)$. The term "(most stable)" refers to the selection made in the Reaction module in FactSage 7.3 thermochemistry software to apply compound phase state changes with temperature. The Reaction module was used with selection of the following databases: FactPS and FToxid. The temperature interval of 1000 °C–2400 °C was used in the calculations to compare the Gibbs free energy lines at the lower temperature of 1350 °C of this work to the much higher temperatures applied in the SAW arc cavity and in the weld pool, typically from 1600 °C liquidus temperature for the carbon steel weld pool up to the high temperatures of 2000 °C–2500 °C in the arc cavity [1,2]. The fluoride species marked as (g) in Fig. 11 remains in the gas phase at 1000 °C–2400 °C. The relative positions of the lines in Fig. 11 indicate the stability order of the metal fluoride species in comparison with the metal of each fluoride. For example, the line for AlF is positioned below the line of TiF_4, indicating that Al metal can displace Ti from TiF_4 to form AlF. Reaction (1) is an unlikely reaction at the low temperature applied here because CaF_2 decomposition requires higher temperatures. The netto reaction in Equation (2) is of interest in this work, and it is obtained as the sum of reactions (3) and (4), which are presented in the Gibbs free energy lines in Fig. 11. The Gibbs free energy for the netto reaction in Equation (2) is then the sum of the Gibbs free energy from the simplified reactions in Equations (3) and (4). This calculation is illustrated in Fig. 12 for the reactions of TiF_4 and SiF_4 with Al. The close position of the lines for TiF_4 and SiF_4 in Fig. 11 indicates that these metal fluorides have similar stability. The Gibbs free energy lines for the netto reaction between Al and these fluorides to form the different Al-fluorides of AlF, AlF_2, and AlF3, are displayed in Fig. 12 and indicate that AlF is most easily formed from the reaction of TiF_4 and SiF_4 with Al for the reaction of pure compounds.

$$M(\text{most stable}) + (x/2)F_2(g) \leftrightarrow MF_X(\text{most stable}) \quad (1)$$

$$yAl + xTiF_y(g) \leftrightarrow xTi + yAlF_x(g) \quad (2)$$

$$yAl + xy/2F_2(g) \leftrightarrow yAlF_x(g) \quad (3)$$

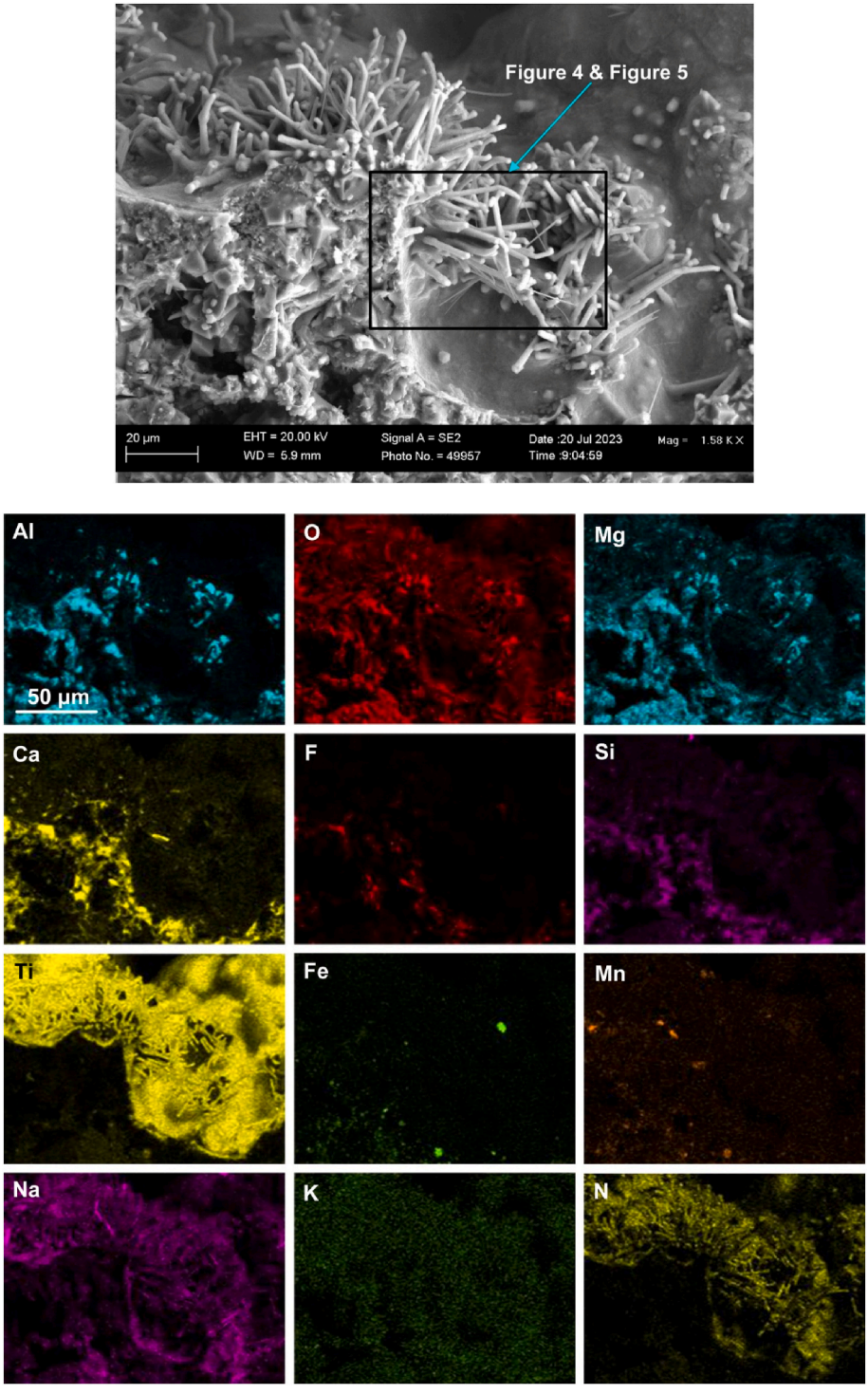

Fig. 3(a). SEM image (x1580) of analysed area as marked in Fig. 2(a); (b): EDS map of area in Fig. 3(a).

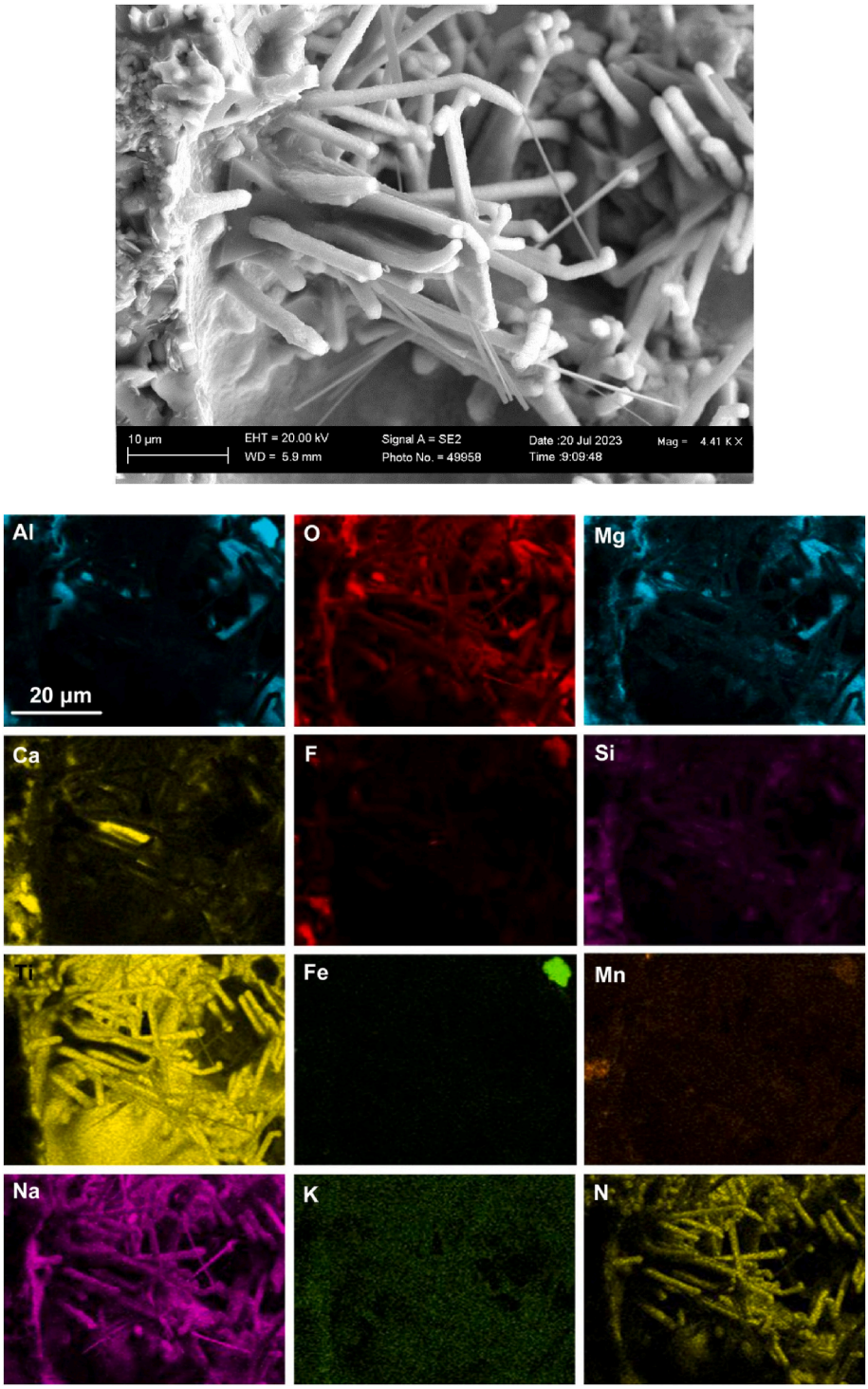

Fig. 4(a). SEM image (x4410) of analysed area as marked in Fig. 3(a); (b): EDS map of area in Fig. 4(a).

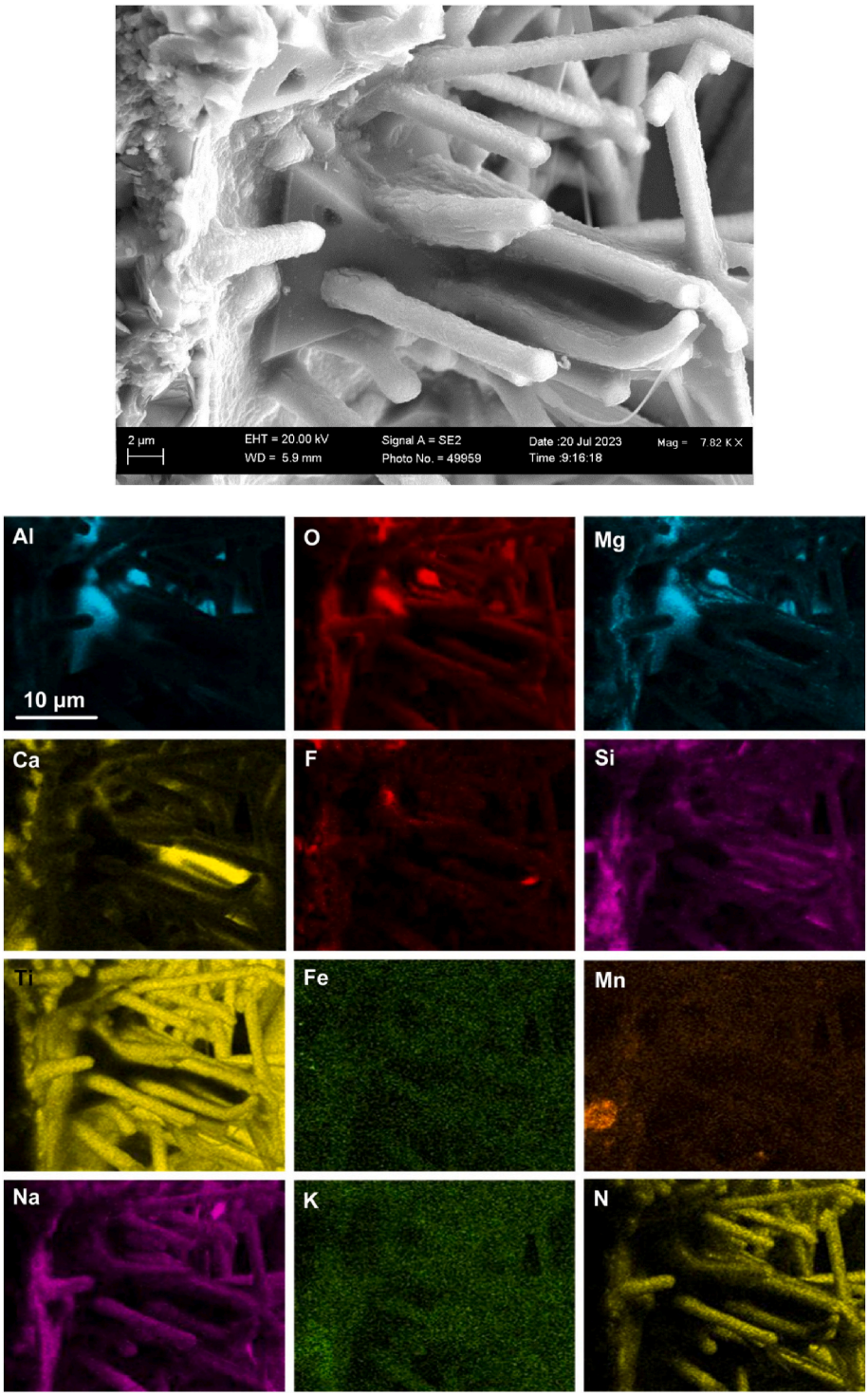

Fig. 5(a). SEM image (x7820) of analysed area as marked in Fig. 3(a); (b): EDS map of area in Fig. 5(a).

$$xTiF_y(g) \leftrightarrow xTi + xy/2F_2(g) \quad (4)$$

In addition, the typical reaction considered in CaF_2-based SAW flux reaction systems is similar to reaction (5), which is the reaction of CaF_2 with an oxide to form alternate fluorides and CaO [3,25].

$$SiO_2(l) + 2CaF_2(g) \leftrightarrow 2CaO(l) + SiF_4(g) \quad (5)$$

Gibbs free energy values for reaction (5) are summarised in Fig. 13. The input conditions were set to 1 atm CaF_2 partial pressure, 0.10 atm partial pressure of product fluoride gas, unit activity liquid flux oxide, and the activity of CaO set to 0.01 ($a_{CaO} = 0.01$). These conditions were selected as a basis of comparison, similar to previous calculations for SAW fluxes [20]. It is seen that SiF_4 is most easily formed below 1380 °C. The lines for the reaction of Na_2O and K_2O with CaF_2 to form NaF and KF cross the line for SiF_4 formation at 1380 °C. The lines for TiF_3 and AlF_3 are slightly sloped across the temperature range in Fig. 13, indicating that TiF_3 formation is relatively more probable than AlF_3 formation, and the relative stability of these two fluoride gasses remains the same from 1000 °C to 2400 °C. Furthermore, the negative Gibbs free energy values

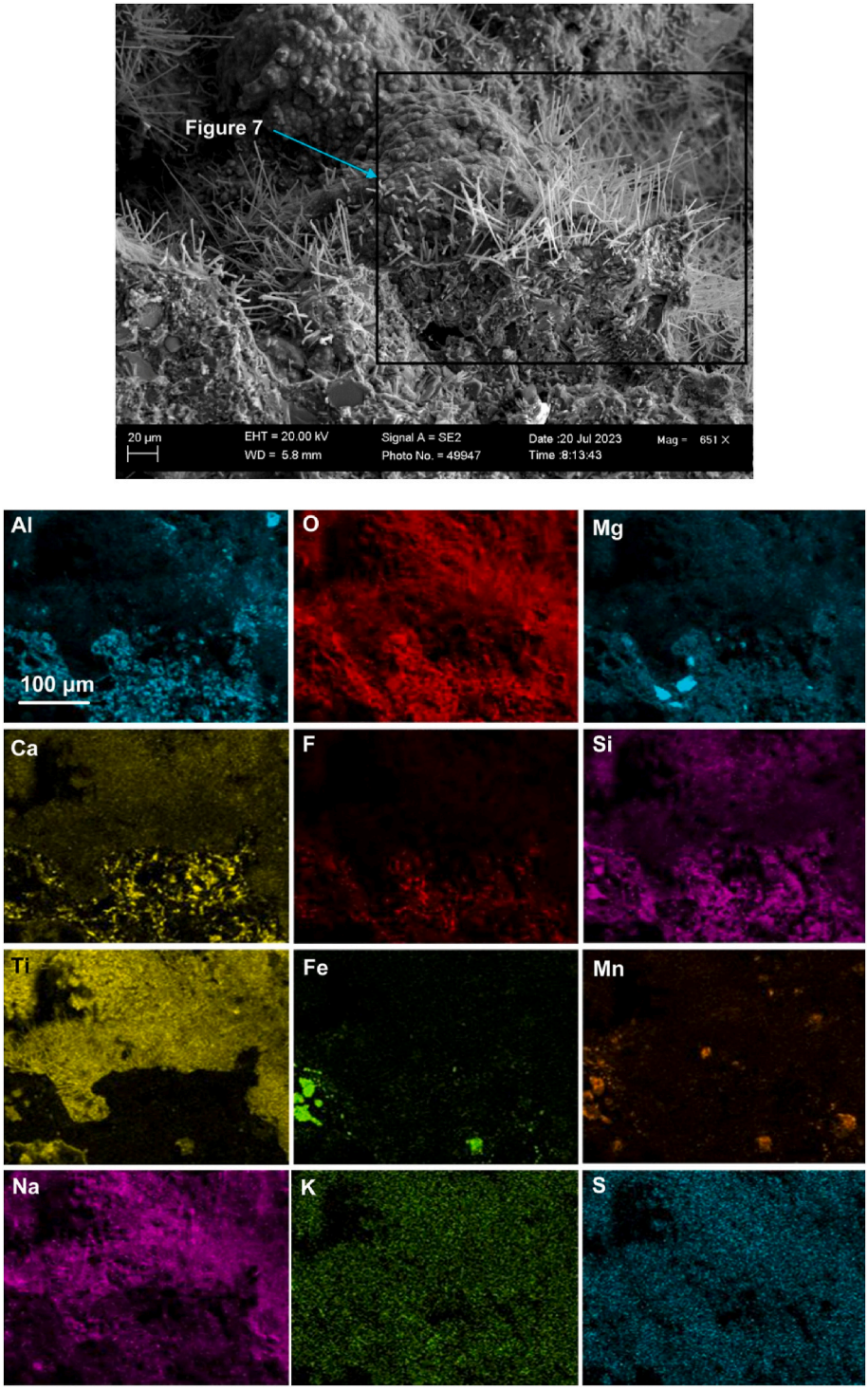

Fig. 6(a). SEM image (x651) of analysed area; (b): EDS map of area in Fig. 6(a).

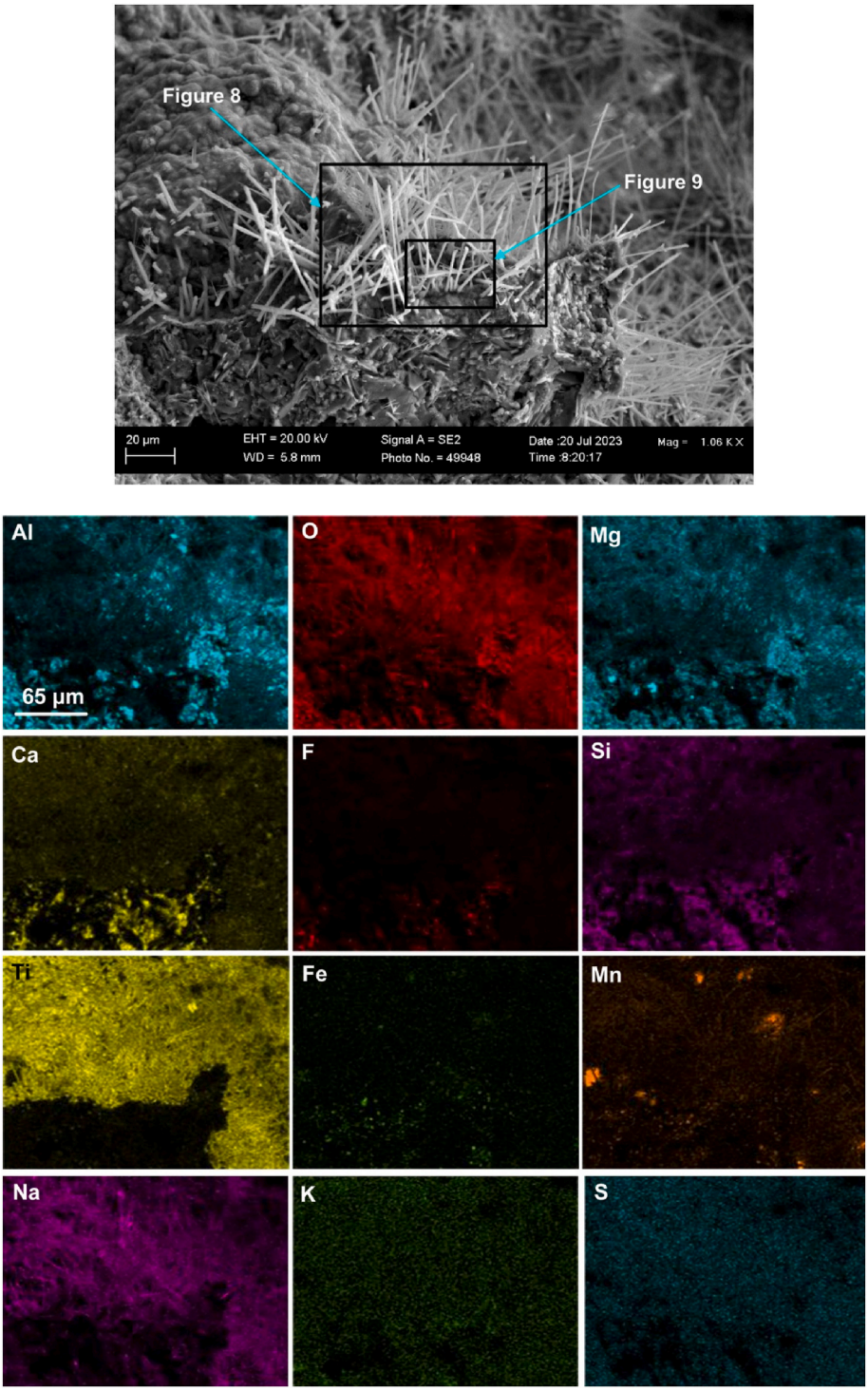

Fig. 7(a). SEM image (x1060) of analysed area as marked in Fig. 6(a); (b): EDS map of area in Fig. 7(a).

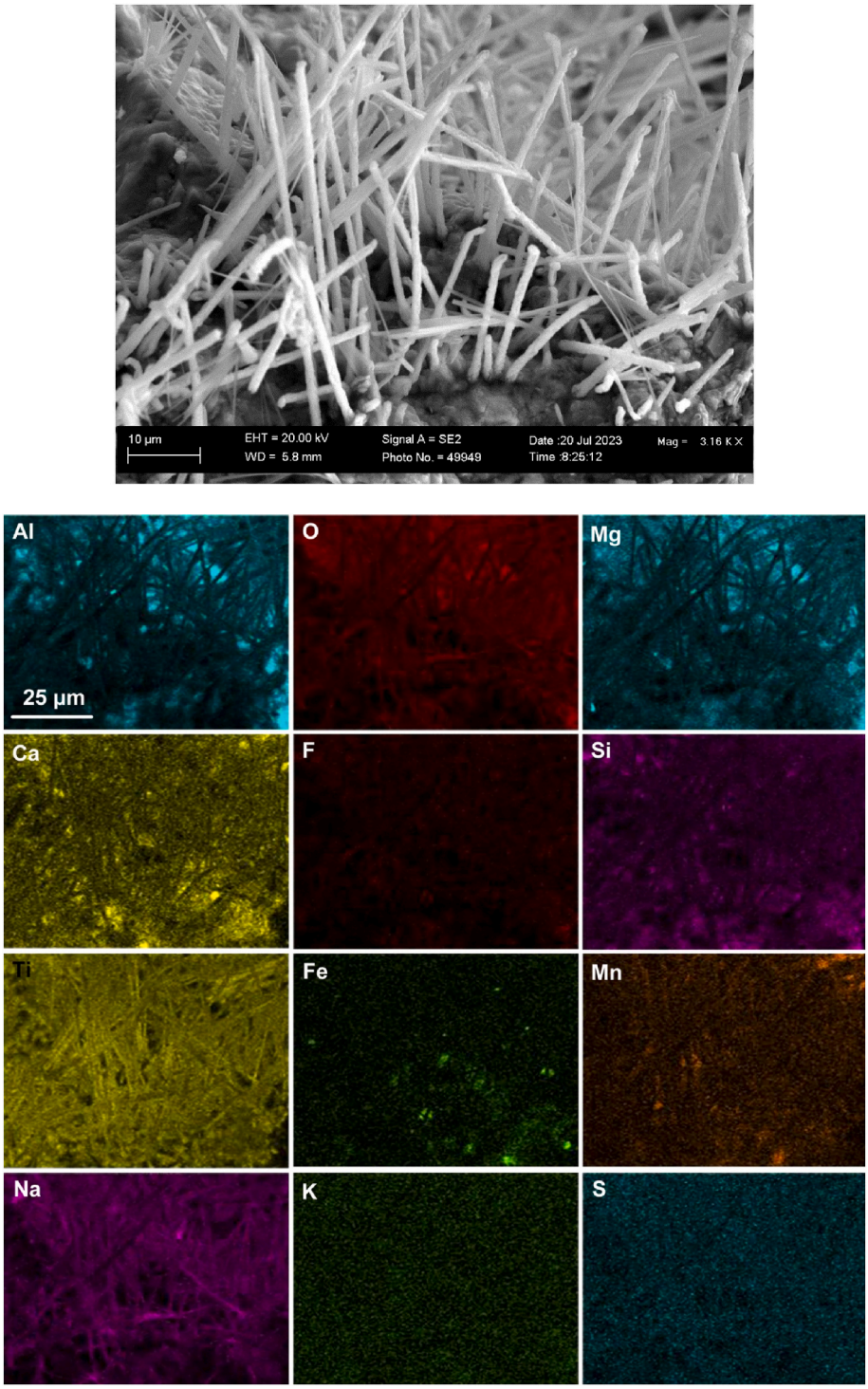

Fig. 8(a). SEM image (x3160) of analysed area as marked in Fig. 7(a); (b): EDS map of area in Fig. 8(a).

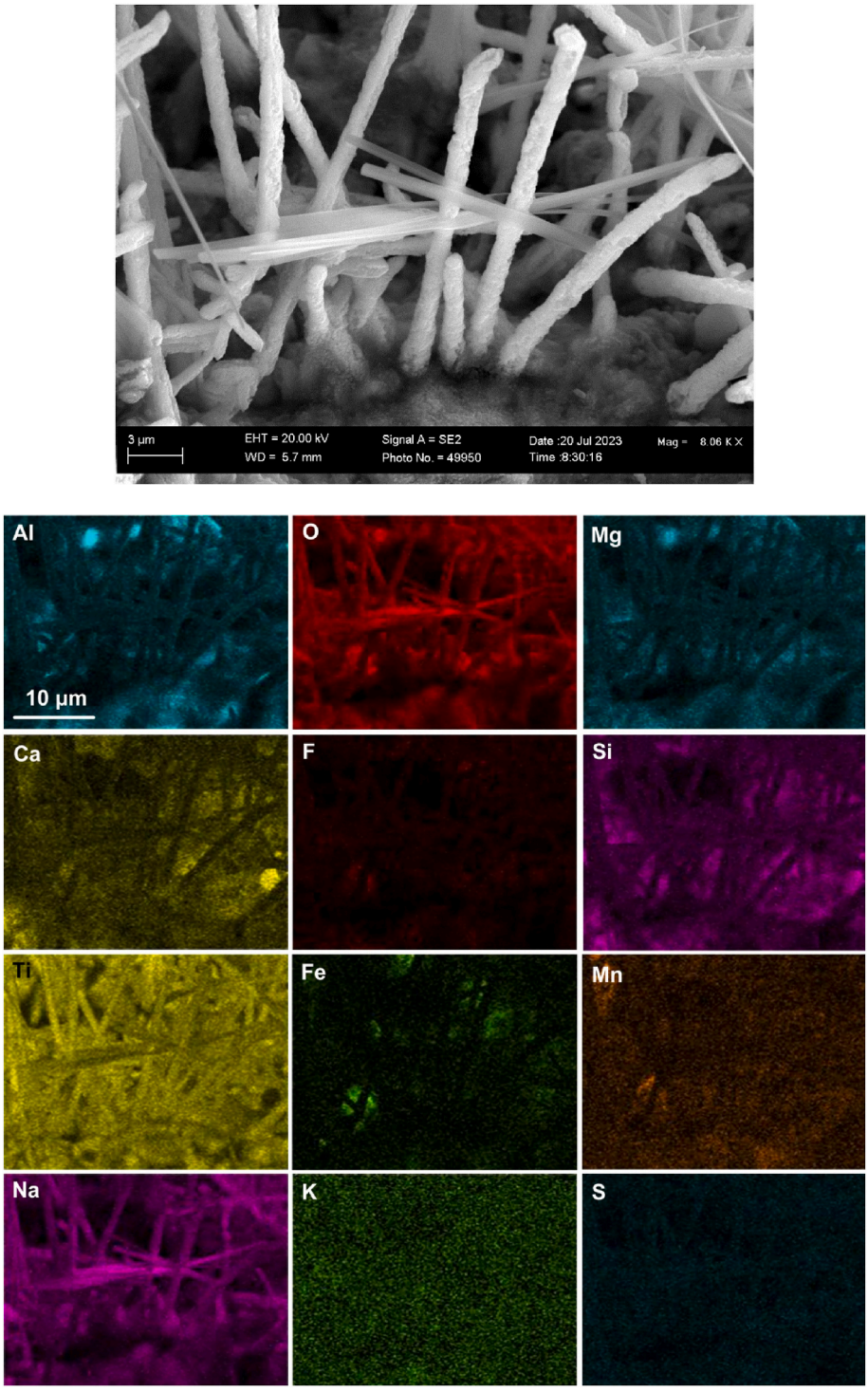

Fig. 9(a). SEM image (x8060) of analysed area as marked in Fig. 7(a)(a); (b): EDS map of area in Fig. 9(a).

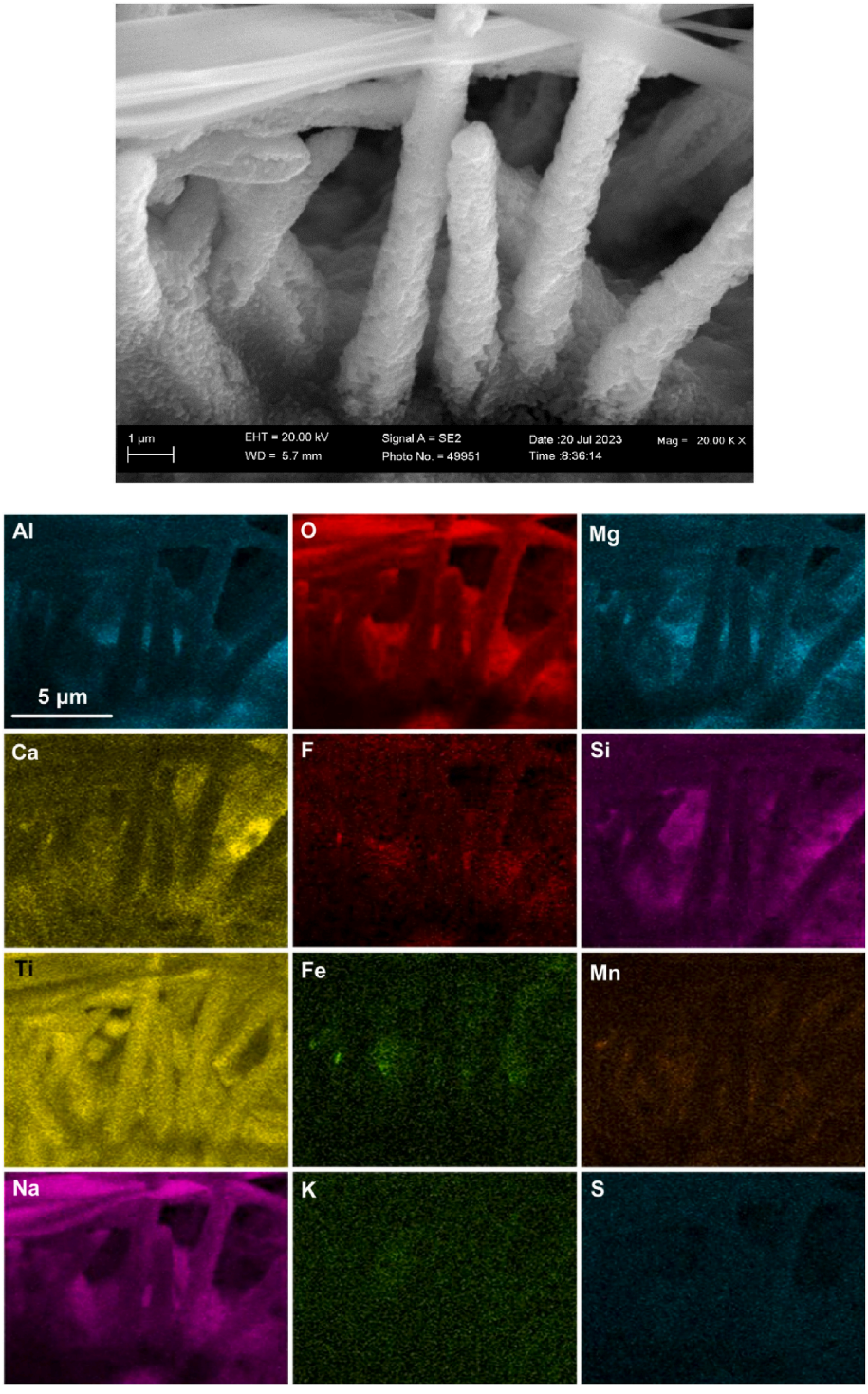

Fig. 10(a). SEM image (x20000) of analysed area; (b): EDS map of area in Fig. 10(a).

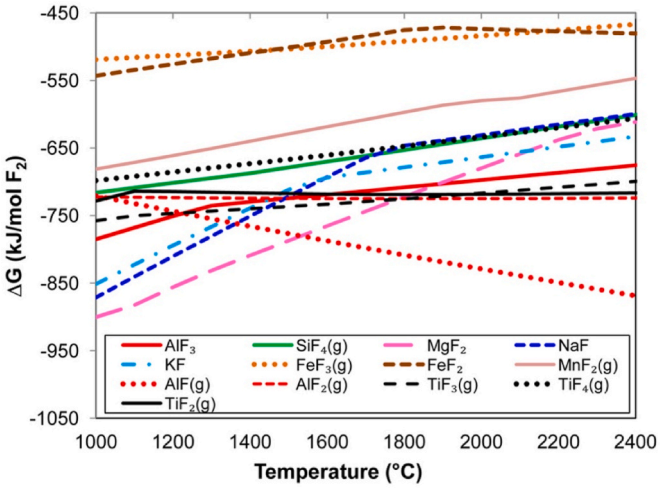

Fig. 11. Gibbs free energy of metal-fluoride formation via reaction (1).

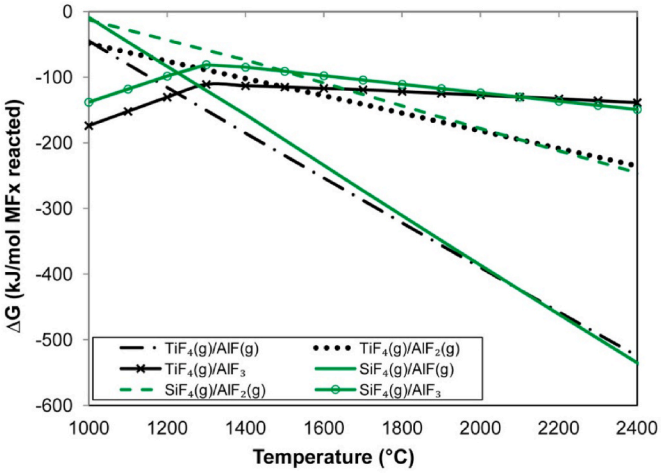

Fig. 12. Gibbs free energy for reaction of Al with TiF_4 and SiF_4.

in Fig. 12 for AlF(g) formation from the reaction of Al with TiF_4 and SiF_4 are significantly larger than those in Fig. 13, meaning that the thermodynamic driving force for metal-based reactions in Equation (2) is higher than that of Equation (3) reactions.

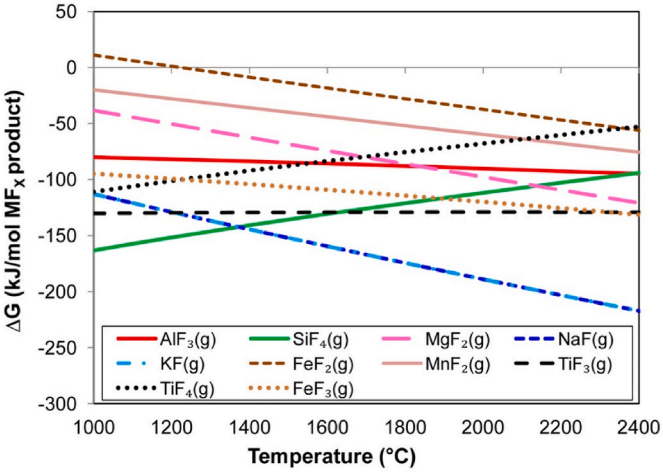

Fig. 13. Gibbs free energy of fluoride formation via reaction (5).

3.2.2. Gas-slag-metal thermochemical calculations

Because the thermochemistry calculations displayed in Figs. 11–13 are for simplified reactions of pure reactants, whilst, in reality, the reactants and products in the reaction system are not pure species, a better simulation of the reaction system should be more insightful. The gas-slag-metal equilibrium model previously developed for SAW process simulation was applied to the reaction system to calculate the likely gas phase species formed at 1350 °C [9].

The simulation calculation was done for 1350 °C at different proportions of Al and Ti metal powders reacted with the flux. The results in Table 3 show the Al addition results in increased Al-fluoride species in the gas, namely $KAlF_4$, $NaAlF_4$ and AlF_3. As Zeitsev et al. [18] discussed, $KAlF_4$ may be regarded as KF and AlF_3, and similarly, $NaAlF_4$ may be presented as NaF and AlF_3. When zero Ti is added (scenario 3), the main gas species are $KAlF_4$ and $NaAlF_4$. With both Al and Ti added to the calculation (scenarios 1 and 2), the gas composition shifts to show increased TiF_3 and some TiF_2 present in the gas in addition to the Al-fluoride species formed from the reaction of Al metal powder with the fluoride flux. At a higher Al/Ti ratio in the metal powders, compare scenario 4 to scenario 1, the proportion of TiF3 in the gas is decreased, indicating the formation of Al-fluoride gas in preference to TiF_3 gas. This effect should diminish the loss of Ti to the gas phase.

The increased oxygen content shown in Table 2 and the association of Ti and O in the nano-strands in Figs. 2(b) to 10(b) raise the question as to how this simultaneous uptake of Ti and O may have occurred. Although the SEM-EDS oxygen analyses are only qualitative, the relative increase in oxy-fluoride oxygen content requires consideration. Work by Zeitsev et al. [18] identified low temperature vaporisation of oxygen-containing fluoride gas in the form of AlOF. Similarly, in the FactSage simulation calculations, small quantities of analogue Ti-containing gas species were calculated, namely OTiF, $OTiF_2$, and TiO and TiO_2. Although these species were calculated for equilibrium conditions, in non-equilibrium conditions such as expected here, these gas phase species may occur in higher concentrations as intermediary species before equilibrium is attained. Similarly, SiO gas forms and may also carry oxygen and silicon into the nano-strands during re-condensation of the fluoride-containing gas. At least at the start of the reaction process, some oxygen is evolved from the Fe_2O_3 present in the flux formulation, and this oxygen may also play a role as an oxygen incorporation mechanism to the nano-strands.

4. Conclusions

- Oxy-fluoride nano-strand formation was identified in the low temperature (1350 °C) reaction of SAW flux and Al, Fe and Ti metal powders.
- Ti and O are extensively incorporated into the nano-strands, confirming that the Ti was assimilated from the added Ti metal powder via the gas phase.
- Ti-fluoride and Al-fluoride gas are easily formed in this reaction system at 1350 °C.
- Thermochemical analysis clarifies the role of Al in shifting the gas phase composition to limit Ti-fluoride loss reactions in the gas phase.
- The low temperature experimental technique applied here serves as an accurate reaction simulation experiment to investigate oxy-fluoride behaviour, gas formation and metal powder assimilation reactions in the SAW process.

CRediT authorship contribution statement

T. Coetsee: Conceptualization, Formal analysis, Investigation, Methodology, Writing – original draft, Writing – review & editing. **F.J. De Bruin:** Conceptualization, Formal analysis, Investigation, Methodology, Writing – review & editing.

Table 3
Gas composition from gas-slag-metal equilibrium model (FactSage 7.3).

Scenario No.	g. Al	g. Ti	%TiF_3	%$KAlF_4$	%$NaAlF_4$	%SiF_4	%TiF_2	%AlF_3	%Na	%SiF_3
1	6	4	39	35	21	2	1	1	0.5	0.3
2	6	2	19	50	23	4	0.5	1	0.3	1
3	6	0	1	59	27	8	0.3	3	0.3	2
4	8	4	7	72	17	1	0.3	1	1	0.2

Declaration of competing interest

The authors declare that they have no known competing financial interests or personal relationships that could have appeared to influence the work reported in this paper.

Data availability

Data will be made available on request.

Acknowledgements

This work was supported in part by the University of Pretoria. The authors are grateful to Erna van Wilpe and Coenraad Snyman at the Laboratory for Microscopy and Microanalysis at the University of Pretoria for their advice and assistance on SEM imaging and analysis in this work.

References

[1] C.S. Chai, T.W. Eagar, Slag-metal equilibrium during Submerged Arc Welding, Metall. Trans. B 12 (1981) 539–547.
[2] U. Mitra, T.W. Eagar, Slag-metal reactions during welding: Part 1. Evaluation and reassessment of existing theories, Metall. Trans. B 22 (1991) 65–71.
[3] C.S. Chai, T.W. Eagar, Slag metal reactions in binary CaF_2-metal oxide welding fluxes, Weld. J. 61 (1982) 229S–232S.
[4] A. Polar, J.E. Indacochea, M. Blander, Electrochemically generated oxygen contamination in submerged arc welding, Weld. J. 69 (1990) 68S–74S.
[5] T. Lau, G.C. Weatherly, A. Mc Lean, The sources of oxygen and nitrogen contamination in Submerged Arc Welding using CaO-Al_2O_3 based fluxes, Weld. J. 69 (1985) 343S–347S.
[6] A. O'Brien, Welding Handbook. Volume 4—Welding Processes, Part 1, ninth ed., American Welding Society (AWS), Miami, FL, USA, 2004, pp. 286–289.
[7] J. Zhang, T. Coetsee, S. Basu, C. Cong, Impact of gas formation on the transfer of Ti and O from TiO_2-bearing basic-fluoride fluxes to submerged arc welded metals: a thermodynamic approach, Calphad 71 (2020) 102195.
[8] J. Zhang, T. Coetsee, H. Dong, C. Cong, Element transfer behaviors of fused CaF_2-TiO_2 fluxes in EH36 shipbuilding steel during high heat input Submerged Arc Welding, Metall. Trans. B 51 (2020) 1953–1957.
[9] T. Coetsee, R.J. Mostert, P.G.H. Pistorius, P.C. Pistorius, The effect of flux chemistry on element transfer in Submerged Arc Welding: application of thermochemical modelling, Mater. Res. Technol. 11 (2021) 2021–2036.
[10] T. Coetsee, F. De Bruin, Reactions at the molten flux-weld pool interface in submerged arc welding, High Temp. Mater. Processes (London, U. K.) 40 (2021) 421–427.
[11] T. Coetsee, F.J. De Bruin, Improved titanium transfer in Submerged Arc Welding of carbon steel through aluminium addition, Miner. Process. Extr. Metall. Rev. 43 (2021) 771–774.
[12] T. Coetsee, F. De Bruin, Insight into the chemical behaviour of chromium in CaF_2-SiO_2-Al_2O_3-MgO flux applied in aluminium-assisted alloying of carbon steel in submerged arc welding, Minerals 12 (2022) 1397.
[13] T. Coetsee, F. De Bruin, Aluminium-assisted alloying of carbon steel in submerged arc welding: application of Al-Cr-Ti-Cu unconstrained metal powders, Processes 10 (2022) 452.
[14] T. Coetsee, F. De Bruin, Chemical behaviour of copper in the application of unconstrained Cr-Ni-Al-Cu metal powders in submerged arc welding: gas phase thermodynamics and 3D slag SEM evidence, Processes 11 (2023) 351.
[15] T. Coetsee, F. De Bruin, EERZ (effective equilibrium reaction zone) model of gas-slag-metal reactions in the application of unconstrained Al-Ni-Cr-Co-Cu metal powders in submerged arc welding: model and 3D slag SEM evidence, Processes 11 (2023) 2110.
[16] T. Schultz, B. Lychatz, N. Haustein, D. Janke, Structurally based assessment of the influence of fluorides on the characteristics of continuous casting powder slags, Metall. Trans. B 44 (2013) 317–326.
[17] J. Gao, G. Wen, Q. Liu, W. Tan, P. Tang, Effect of Al_2O_3 on the fluoride volatilization during melting and ion release in water of mould flux, J. Non-Cryst. Solids 409 (2015) 8–13.
[18] A.I. Zaitsev, A.V. Leites, A.D. Litvina, B.M. Mogutnov, Investigation of the mould powder volatiles during continuous casting, Steel Res. 65 (1994) 368–374.
[19] J. Ju, G. Ji, J. An, C. Tang, Effect of TiO_2 on fluoride evaporation from CaF_2-$CaOAl_2O_3$-MgO-Li_2O-(TiO_2) slag, Ironmak. Steelmak. 48 (2020) 109–115.
[20] T. Coetsee, Phase chemistry of Submerged Arc Welding (SAW) fluoride based slags, Mater. Res. Technol. 9 (2020) 9766–9776.
[21] C.W. Bale, E. Bélisle, P. Chartrand, S. Decterov, G. Eriksson, A.E. Gheribi, K. Hack, I.-H. Jung, Y.-B. Kang, J. Melançon, et al., Reprint of: FactSage thermochemical software and databases, 2010–2016, Calphad 55 (2016) 1–19.
[22] T. Coetsee, F. De Bruin, In situ modification of CaF_2-SiO_2-Al_2O_3-MgO flux applied in the aluminium-assisted transfer of titanium in the submerged arc welding of carbon steel: process mineralogy and thermochemical analysis, Minerals 12 (2022) 604.
[23] D.R. Poirier, G.H. Geiger, Transport Phenomena in Materials Processing, TMS, Warrendale PA, USA, 1994.
[24] E.T. Turkdogan, Fundamentals of Steelmaking, The Institute of Materials, Cambridge, UK, 1996.
[25] T. Lau, G.C. Weatherly, A. Mc Lean, Gas/Metal/Slag reactions in Submerged Arc Welding using CaO-Al_2O_3 based fluxes, Weld. J. 70 (1986) 31S–38S.